EBioMedicine 53 (2020) 102701

Contents lists available at ScienceDirect

EBioMedicine

journal homepage: www.elsevier.com/locate/ebiom

Research paper

Microtubule associated protein 9 inhibits liver tumorigenesis by suppressing ERCC3

Jing Zhang[a,b], Jun-Zhe Huang[a], Yan-Quan Zhang[a], Xiang Zhang[a], Liu-Yang Zhao[a], Chuan-Gen Li[a], Yun-Fei Zhou[a], Hong Wei[c], Jun Yu[a,*]

[a] Institute of Digestive Disease and Department of Medicine and Therapeutics, State Key Laboratory of Digestive Disease, Li Ka Shing Institute of Health Sciences, Shenzhen Research Institute, The Chinese University of Hong Kong, Hong Kong
[b] Department of Gastroenterology, Shanghai Jiao Tong University Affiliated Sixth People's Hospital, Shanghai, China
[c] Center of Precision Medicine, The First Affiliated Hospital, Sun Yat-sen University, Guangzhou, China

ARTICLE INFO

Article History:
Received 4 September 2019
Revised 4 February 2020
Accepted 17 February 2020
Available online xxx

Keywords:
Microtubule associated protein 9
Promoter methylation
Hepatocellular Carcinoma
ERCC3

ABSTRACT

Background: Chromosomal instability plays an important part in cancer, but its genetic basis in liver tumorigenesis remains largely unclear. We aimed to characterize the mechanistic significance and clinical implication of mitotic regulator microtubule-associated protein 9 (MAP9) in hepatocellular carcinoma (HCC).
Methods: The biological functions of MAP9 were determined by in vitro tumorigenicity assays. Systematic MAP9 knockout mouse ($MAP9^{\Delta/\Delta}$) and hepatocyte-specific MAP9 knockout mouse ($MAP9^{\Delta/\Delta hep}$) were generated to confirm the role of MAP9 in HCC. The clinical impact of MAP9 was assessed in primary HCC tissue samples.
Findings: We found that MAP9 was frequently silenced in HCC tissue samples. The transcriptional silence of MAP9 in liver cancer cell lines and tissue samples was mediated by its promoter hypermethylation. MAP9 promoter hypermethylation or downregulation was associated with poor survival and recurrence in patients with HCC. Mechanistically, ectopic expression of MAP9 in LO2 and HepG2 cell lines impaired cell proliferation, colony formation, migration and invasion, and induced cell apoptosis and cycle arrest, whereas knockdown of MAP9 in Miha cell line showed the opposite effects. We found that $MAP9^{\Delta/\Delta}$ mice spontaneously developed a liver hyperplastic nodule and $MAP9^{\Delta/\Delta hep}$ accelerated diethylnitrosamine-induced HCC formation. The tumour suppressive effect of MAP9 in HCC was mediated by downregulating excision repair cross-complementation group 3 (ERCC3), a nucleotide excision repair gene. Restoration of ERCC3 expression possessed an oncogenic potency and abrogated the tumour suppressive effects of MAP9.
Interpretation: MAP9 is a novel tumour suppressor in HCC by inhibiting ERCC3 expression, and serves as a prognostic factor in HCC patients.

1. Introduction

Hepatocellular carcinoma (HCC) remains one of the most common malignancies with an increased incidence and ranks as the second-leading cause of cancer-related deaths worldwide [1,2]. In spite of the improvements in surgical and adjuvant treatment strategies, HCC is still a devastating disease with a poor prognosis. Epigenetic dysregulation exerts a critical role in human cancer and the inactivation of tumour suppressor genes by promoter hypermethylation has been involved in the initiation and pathogenesis of HCC [3,4]. Identification of novel epigenetically modified tumour suppressor genes may provide new targets for the diagnosis and treatment of HCC. Using a genome-wide methylation microarray analysis in primary HCC tissue samples, microtubule-associated protein 9 (MAP9) was identified to be substantially hypermethylated in HCC.

MAPs exhibit a variety of functions implicated in influencing the dynamics of the microtubule cytoskeleton [5]. Recent studies indicated that alterations in MAPs are associated with human cancers [6–8]. MAP9, located on chromosome 4q32.1, is responsible for spindle assembly and cytokinesis [9], and enriched in vertebrate brain and testis tissues [10], but its deficiency gives rise to zebrafish embryo developmental defects [11]. In response to DNA damage, MAP9 accelerates p53 transcription by increasing p300-mediated acetylation and decreasing MDM2-mediated ubiquitination [12]. A recent study reported that MAP9 is downregulated in colorectal and breast cancers and can be utilized as a disease marker [13]. To date, the functional importance and molecular mechanisms of MAP9 in HCC are still unknown.

* Corresponding author.
E-mail address: junyu@cuhk.edu.hk (J. Yu).

https://doi.org/10.1016/j.ebiom.2020.102701

Research in Context

Evidence before this study

➢ Hepatocellular carcinoma (HCC) is one of the most common malignancies worldwide.
➢ Microtubule associated protein 9 (MAP9), located on chromosome 4q32.1, is a gene responsible for spindle assembly and cytokinesis.
➢ MAP9 was identified to be hypermethylated in HCC using a genome-wide methylation microarray analysis in primary HCC tissues.

Added value of this study

➢ MAP9 is frequently silenced or downregulated in liver cancer due to promoter hypermethylation.
➢ MAP9 promoter hypermethylation is an independent prognostic factor of poor survival and tumour recurrence in patients with HCC.
➢ MAP9 acts as a tumour suppressor in HCC through inducing apoptosis escape and cell cycle progression and reviving invasive potential through upregulating ERCC3 expression.
➢ Knockout of MAP9 in mice elicited spontaneous liver hyperplastic nodule formation and hepatocyte-specific MAP9 knockout facilitated diethylnitrosamine (DEN)-induced HCC.

Implications of all the available evidence

➢ MAP9 is a novel tumour suppressor in HCC by inhibiting ERCC3 expression.
➢ Detection of methylated MAP9 may serve as a new biomarker for the prognosis of patients with HCC.

In the present study, we identified that MAP9 was commonly silenced in liver cancer cell lines and tissue samples due to its promoter hypermethylation. MAP9 promoter hypermethylation harboured a robust association with poor survival and tumour recurrence in patients with HCC. Moreover, knockout of MAP9 ($MAP9^{\Delta/\Delta}$) in mice elicited spontaneous liver hyperplastic nodule formation and hepatocyte-specific MAP9 knockout ($MAP9^{\Delta/\Delta hep}$) facilitated diethylnitrosamine (DEN)-induced hepatocarcinogenesis. Mechanistically, loss of MAP9 expression promoted liver cancer cell growth by inducing apoptosis escape and cell cycle progression and reviving invasive potential through upregulating ERCC3 expression.

2. Materials and methods

2.1. Cell lines and human samples

Seven liver cancer cell lines (Hep3B, HepG2, PLC5, SNU-423, SK-hep, Huh6 and Huh7) and two immortalized human liver cell lines LO2 and Miha were used in this study. Hep3B, HepG2, PLC5 and SNU-423 cell lines were obtained from the American Type Culture Collection Cell Bank. Huh6 and Huh7 cell lines were obtained from Japanese Collection of Research Bioresources Cell Bank. LO2 cell line was obtained from Culture centre of institute of basic medical sciences, Chinese academy of medical sciences (Beijing, China) and Miha cell line was donated by Dr. J.R. Chowdhury, Albert Einstein College of Medicine (New York, USA). All the cell lines were routinely cultured in Dulbecco's modified Eagle's medium (DMEM, Gibco BRL, Rockville, MD) supplemented with 10% foetal bovine serum (Gibco BRL).

Paired primary HCC tissue samples (n = 64) were collected immediately after surgical resection from the Third Affiliated Hospital of Sun Yat-Sen University (Guangzhou, China) and the patients were follow up from July 24th 2012 to November 29th 2013. The specimens were snap-frozen in liquid nitrogen and stored at −80 °C. All liver cancer patients signed the informed consent, and the study protocol was approved by the Clinical Research Ethics Committee of the Sun Yat-Sen University (Guangzhou, China).

2.2. Tissue microarray and immunohistochemistry

Tissue microarray (TMA), which was generated from formalin-fixed and paraffin-embedded archived tissue samples of 22 patients with liver cancer prior to radiotherapy or chemotherapy, was purchased from Shanghai Outdo Biotech Co., LTD (Shanghai, China). Immunohistochemistry (IHC) for MAP9 was performed on paraffin sections of TMA using anti-MAP9 antibody (HPA037864, 1:200, Sigma-Aldrich). The extent of MAP9 cytoplasmic staining was evaluated by H-score, as previously described [14]. IHC analysis of Ki-67 levels was also conducted on paraffin slides of mouse liver and tumour tissues using anti-Ki-67 antibodies (Abcam, Cambridge, UK).

2.3. Data mining in the cancer genome atlas (TCGA)

In TCGA-liver cancer, the data regarding paired liver cancer samples (n = 50), and 260 cases of patients with liver cancer including intact overall survival and recurrence time and status, MAP9 or ERCC3 expression level (RNA-seq), MAP9 DNA methylation level (Illumina 450k Infinium methylation beadchip), age, gender, HBV/HCV infection, liver fibrosis, tumour differentiation, pathological stage, TNM staging, tumour size and distant metastasis were downloaded by using the UCSC Xena browser (https://xenabrowser.net/heatmap/).

2.4. RNA extraction and real-time PCR analysis

Total RNA was extracted using TRIzol and transcribed into cDNA using a High Capacity cDNA Kit (Applied Biosystems, Foster City, CA). For quantitative PCR analysis, aliquots of cDNA were amplified using SYBR® Premix Ex Taq™ II (Takara Bio Inc, Japan) on LightCycler® 480 Instrument (Roche Diagnostics, Switzerland). Each sample was tested in triplicate. $2^{-\Delta\Delta CT}$ method was employed to evaluate the fold change in gene expression level. $2^{-\Delta CT}$ method was employed to determine the relative expression levels of corresponding genes. The sequences of primers used were listed in Supplementary Table S1.

2.5. Western blot analysis

Protein lysates from cell lines and tissues were prepared using protease inhibitor cocktail (Roche)–containing radioimmunoprecipitation assay (RIPA) buffer. Protein concentration was determined by the DC protein assay method of Bradford (Bio-Rad, Hercules, CA). Proteins were separated on sodium dodecyl sulfate-polyacrylamide gel electrophoresis (SDS-PAGE) and transferred onto nitrocellulose membranes (GE Healthcare, Piscataway, NJ). Blots were immunostained with primary antibodies at 4 °C overnight and secondary antibody at room temperature for 1 h. Proteins were visualized using ECL Plus Western Blotting Detection Reagents (GE Healthcare). The antibodies used in this study were listed in Supplementary Table S2.

2.6. Bisulfite treatment of DNA and methylation-specific PCR (MSP) analysis

Genomic DNA was extracted from liver cancer samples and cell lines and then was subjected to bisulfite treatment using CpGenome DNA Modification Kit (Chemicon, USA). The sequences of primers were indicated in Supplementary Table S1. The band expanded with MSP primers corresponding to the DNA methylation in the promoter

region was marked as "M". The band expanded with non-methylation specific primers was marked as "U".

2.7. Bisulfite genomic sequencing (BGS)

The PCR products of bisulfite-treated DNA were cloned into the pCR4-Topo vector (Life Technologies, Carlsbad, CA). 10 colonies were randomly chosen and sequenced. Sequencing analysis was performed by SeqScape software (Applied Biosystems, Foster City, CA) and 11 CpG sites spanning in the promoter region of 224 bp were assessed.

2.8. Demethylation treatment

1×10^6 cells were placed in 100-mm dishes and grown for 24 h. Cells were then treated with 10 μM of 5-aza-2′-deoxycytidine (5-Aza) (Sigma-Aldrich, St Louis, MO) for 48 h. Culture medium containing 5-Aza was replenished every day.

2.9. Construction of gene expression plasmid

The full-length open reading frame sequence of MAP9 or ERCC3 was obtained by RT-PCR amplification of normal human liver cDNA. The PCR aliquots were subcloned into the mammalian expression vector pcDNA3.1 and then verified by DNA sequencing. Overexpression of MAP9 or ERCC3 in LO2 or HepG2 cells was transfected with pcDNA3.1, pcDNA3.1-MAP9 or ERCC3 plasmid using lipofectamine 2000 (Life Technologies). Stable transfections were selected for 2 weeks with G418 antibiotics.

2.10. RNA interference and transfection

Knockdown of MAP9 expression in Miha cell line was performed by a siRNA targeting MAP9. Miha cell line were transfected with 20 nM MAP9 siRNA (siMAP9: 5′-GAG CUA AUA AGA GCA AUU ATT-3′) (Shanghai, GenePharma) or control siRNA (siNC: 5′-UUC UCC GAA CGU GUC ACG UTT −3′) (Shanghai, GenePharma) using lipofectamine 2000. After transfection for 48 h., the cells were ready for further experiments.

2.11. Cell viability assay

Cell viability was examined by the MTT (3-[4,5-*dimethylthiazol*-2-*yl*]−2,5 diphenyl tetrazolium bromide) assay (Promega, Fitchburg, WI). The experiments were performed three times independently. Results were shown as the means ± SD.

2.12. Colony formation assay

For overexpression assay, LO2 and HepG2 cells (2×10^3 cells/well) were transfected with MAP9, ERCC3 or empty vector and were plated in a 6-well plate. For knockdown assay, Miha cells were transfected with siMAP9 or siNC. After culturing for 7−10 days, cells were fixed with methanol and stained with crystal violet solution. Colonies with >50 cells per colony were counted. All experiments were conducted three times in triplicates.

2.13. Cell apoptosis analysis

Cell apoptosis was determined by staining cells with Annexin V and 7-amino-actinomycin D (7-AAD) (BD Biosciences) with subsequent flow cytometry analysis. Cell populations were counted as viable (Annexin V-negative, 7-AAD-negative), early apoptotic (Annexin V-positive, 7-AAD-negative), late apoptotic (Annexin V-positive, 7-AAD-positive), or necrotic (Annexin V-negative, 7-AAD-positive). The experiments were conducted three times in triplicates. In addition, terminal deoxynucleotidyl transferase-mediated nick-end labelling (TUNEL) assay (Roche) was employed for apoptosis measurement of liver or liver tumour biopsies in mice. Nuclei with clear brown staining were regarded as TUNEL-positive apoptotic cells. The apoptosis index was calculated as the percentage of TUNEL-positive nuclei after counting at least 1000 cells.

2.14. Cell cycle analysis

LO2 and HepG2 cells that were transfected with MAP9 or empty vector were plated in a 6-well plate, while MIha cells were transfected with siMAP9 or siNC. After 48 h of transfection, the cells were fixed in ice-cold 70% ethanol-phosphate-buffered saline for 24 h before staining with 50 μg/ml propidium iodide (BD Biosciences, Franklin Lakes, NJ). The cells were sorted by BD Accuri™ C6 (BD Biosciences), and cell cycle distributions were analysed using the ModFitLT 4.1 software (Verity Software House, Topsham, ME). All experiments were conducted three times in triplicates.

2.15. Wound-healing assay

Cell migration was assessed using the wound-healing assay. Briefly, LO2 and HepG2 cells transfected with pcDNA3.1 or pcDNA3.1-MAP9 were cultured in six-well plates. When the cells reached 80% confluence, three scratch wounds in each well were made using a P-200 pipette tip. Fresh medium supplemented with reduced (5%) foetal bovine serum was then added, and the wound-closure was observed for 72 h. Photographs were taken at 0, 24, 48 and 72 h, respectively.

2.16. Migration and invasion assays

For migration and invasion assays, migration transwell chambers and matrigel-coated chambers (Becton Dickinson, Waltham, MA, USA) were used. Briefly, 5×10^4 cells were seeded into the upper chamber in serum-free culture medium. The lower chamber was filled with completed medium with 10% FBS. After 16 h for migration assay and 24 h for invasion assay, cells that have migrated or invaded through the membrane were stained with crystal violet and counted.

2.17. Immunofluorescence

Cells were seeded onto coverslips in a 6-well plate and transfected with pcDNA3.1 or pcDNA3.1-MAP9. After transfection for 48 h, cells were fixed with 4% paraformaldehyde and permeabilized with 0.2% Triton X-100, blocked in 5% BSA in PBS, and incubated with anti-MAP9 (1:200 dilution, sc-164,961, Santa Cruz) and anti-XPB (1:40 dilution, AB27317, Abcam) overnight at 4 °C, followed by IgG secondary antibody conjugated with Alexa Fluor 594 (1:400 dilution, Yeasen) in the dark for 1 h Cells were then mounted with ProLong Gold Antifade Mountant with DAPI (Life Technologies). Images were captured using a Carl Zeiss LSM 780 confocal laser scanning microscope (Carl Zeiss AG).

2.18. RT2 profiler™ PCR array

Mouse Cancer PathwayFinder RT2 Profiler™ PCR array (PAMM-033ZC, QIAGEN, USA) was utilized for quantitative PCR with the following cycling conditions: 10 min at 95 °C, 15 s at 95 °C, and 1 min 60 °C for 40 cycles with a final 4 °C hold. Five endogenous control genes, namely, glucuronidase β, hypoxanthine guanine, heat-shock protein 90, glyceraldehyde phosphate dehidrogenase, and β-actin, were used for data normalization. Each replicate cycle threshold (CT) was normalized to the average Ct value of five endogenous controls per plate. Results were calculated using the $2^{-\Delta\Delta CT}$ method. Heat map was generated using the web-based program of RT2 Profiler™

PCR array data analysis. Variations in the tumour gene expression between MAP9 knockout mice and wild type mice are shown as a fold of increase or decrease.

2.19. MAP9 knockout ($MAP9^{\Delta/\Delta}$) mouse model

MAP9 knockout ($MAP9^{\Delta/\Delta}$) mice were generated by working with Beijing Biocytogen Co., Ltd (Beijing, China). A targeted vector was electroporated into embryonic stem cells with C57BL/6 background to generate a recombined MAP9 allele (fl-neo). Following selection and identification by PCR and southern blot, positive clones were injected into mouse blastocysts to generate chimaeric mice, which were crossed with Rosa26-Flpe mice (B6.129S4-Gt (ROSA)26Sor $^{tm1(FLP1)Dym}$) [15] to delete the eGFP and neomycin cassette to obtain the floxed allele (fl) mice with Flp recombinase transgene, and the offspring were further crossed with wild-type (WT) C57BL/6 mice to remove Flp recombinase transgene. To gain hepatocyte-specific depletion of MAP9 ($MAP9^{\Delta/\Delta hep}$), fl mice were crossed with hepatocyte-specific Alb-cre mice (Speer6-ps1$^{Tg(Alb\text{-}cre)21Mgn}$) [16] to obtain $MAP9^{\Delta/\Delta}$Alb-Cre/Alb-Cre mice. MAP9 $^{\Delta/\Delta hep}$ and its wild-type littermates were confirmed by PCR genotyping. All animal studies were conducted in accordance with guidelines and approved by the Animal Experimentation Ethics Committee of the Chinese University of Hong Kong.

2.20. DEN-induced liver tumorigenesis in mice

To induce hepatocarcinogenesis, $MAP9^{\Delta/\Delta hep}$ mice and WT mice were singly injected i.p. at 2 weeks of age with 5 mg/kg DEN (Sigma-Aldrich) and were sacrificed at the age of 30 weeks. For all experiments, only male mice were used.

2.21. Hematoxylin and eosin (H&E) staining

Mice livers were harvested and fixed in 4% paraformaldehyde, and preserved in optimal cutting temperature compound. The liver tissues were sliced in 5 μm sections and stained with H&E for the histological studies.

2.22. Statistical analysis

All the results were indicated as mean ± SD. Statistical analysis was conducted using GraphPad Prism version 6.0 (GraphPad Software) or Statistical Package for the Social Sciences (SPSS) (standard V.20.0) (IBM Corporation, New York, USA). The Pearson correlation coefficient was used to assess the correlation of MAP9 expression with its promoter methylation in the clinical samples. The Chi-square test or Fisher exact test was utilized for comparison of patient clinicopathologic characteristics and MAP9 expression or its promoter methylation level. Kaplan-Meier analysis and log-rank test were used to estimate the association of MAP9 methylation or its low expression with overall survival and tumour recurrence. Cox proportional hazards regression model was used to evaluate the prognostic value of MAP9 methylation or its low expression. Mann-Whitney U test or Student's t-test was performed to compare the variables of two groups. P value < 0.05 were considered as statistical significance.

3. Results

3.1. MAP9 is commonly silenced in liver cancer cell lines and tissue samples

We examined MAP9 mRNA expression in 64 paired human HCC tissue samples and found that MAP9 mRNA levels were dramatically decreased in HCC tissues as compared with their adjacent non-tumour tissues, and downregulation of MAP9 mRNA was confirmed in 367 HCC tissues compared with 50 non-tumour tissues from TCGA dataset (Fig. 1a and Supplementary Fig. S1). Accordingly, MAP9 protein expression was found significantly reduced in HCC tissues (89.47±10.68) as compared with adjacent non-tumour tissues (131.00±4.71) by IHC analysis (Fig. 1b). Moreover, MAP9 was silenced in all 6 liver cancer cell lines (Huh6, Huh7, SNU-423, PLC5, SK-Hep1, and HepG2), but readily expressed in normal liver tissues as shown by RT-PCR and Western Blot analysis (Fig. 1c and c2). The immortalized hepatocyte cell line Miha showed MAP9 mRNA and protein expression, but LO2 was silenced (Fig. 1c1 and c2). We investigated the underlying mechanisms of the transcriptional silence of MAP9 by assessing its promoter methylation by methylation-specific PCR (MSP) and bisulfite genomic sequencing (BGS), and found an inverse correlation of MAP9 silence with its promoter hypermethylation in HCC cell lines and primary HCC tissues (Fig. 1c-e). The promoter methylation levels of MAP9 were significantly higher in HCC tissues than those in adjacent non-tumour tissues in our cohort ($P < 0.0001$, paired t-test) and TCGA cohort ($P < 0.01$, paired t-test), and showed a negative correlation with MAP9 mRNA expression in HCC tissues (Fig. 1f). De-methylation treatment by 5-Aza-20- deoxycytidine (5-Aza) could restore the expression of MAP9 in silenced HCC cell lines (Fig. 1g), suggesting that the transcriptional silence of MAP9 is mediated by its promoter hypermethylation in HCC.

3.2. MAP9 promoter hypermethylation is an independent predictor of poor prognosis in HCC patients

To assess the association of MAP9 methylation with the clinicopathological characteristics and prognosis of HCC patients, we measured the MAP9 promoter methylation status in 64 HCC patients from our cohort and 260 HCC patients from TCGA cohort. MAP9 hypermethylation was detected in 26.56% (17/64) of HCC tissues in our cohort as well as in 27.69% (72/260) of HCC tissues in TCGA cohort (Supplementary Table S3). As demonstrated by Kaplan-Meier analysis, HCC patients with MAP9 hypermethylation had a significantly shorter survival in both our cohort and TCGA cohort ($P < 0.001$, Fig. 2a). MAP9 hypermethylation was also associated with liver fibrosis, Tumour-Node-Metastasis (TNM) staging and distant metastasis in our cohort (Supplementary Table S3). By univariate Cox regression analysis, we found that MAP9 hypermethylation was associated with a poor survival in both our cohort (HR 15.729, 95%CI 6.248 to 39.597, $P < 0.0001$) and TCGA cohort (HR 2.136, 95%CI 1.396 to 3.267, $P < 0.0001$) (Fig. 2b). As expected, the TNM stage, metastasis and tumour size were also prognostic factors (Fig. 2b). After adjustment for potential confounding factors including age, gender and TNM stage, MAP9 hypermethylation in these two cohorts was found to be an independent prognostic factor of poor survival in HCC patients by multivariate Cox regression analysis (Fig. 2c). In addition, MAP9 hypermethylation was associated with tumour recurrence (Supplementary Fig. S2a). Univariable and Multivariate Cox regression analysis unveiled MAP9 hypermethylation as an independent prognostic factor of tumour recurrence in HCC patients (Supplementary Fig. S2b). Moreover, MAP9 low expression is a predictor of overall survival of HCC patients in both our cohort and TCGA cohort (Supplementary Table S4, 5) and tumour recurrence in TCGA cohort (Supplementary Table S6).

3.3. MAP9 inhibits liver cancer cell growth through inducing apoptosis and reducing cell cycle progression

We evaluated the functional role of MAP9 in HCC cell lines by generating two stably transfected cell lines (LO2 and HepG2) with MAP9 overexpression and siMAP9-transfected Miha cell line with loss of MAP9 function (Fig. 3a and Supplementary Fig. S3). The number of colonies formed in MAP9-transfected LO2 and HepG2 cell lines was substantially decreased as compared with the empty vector-

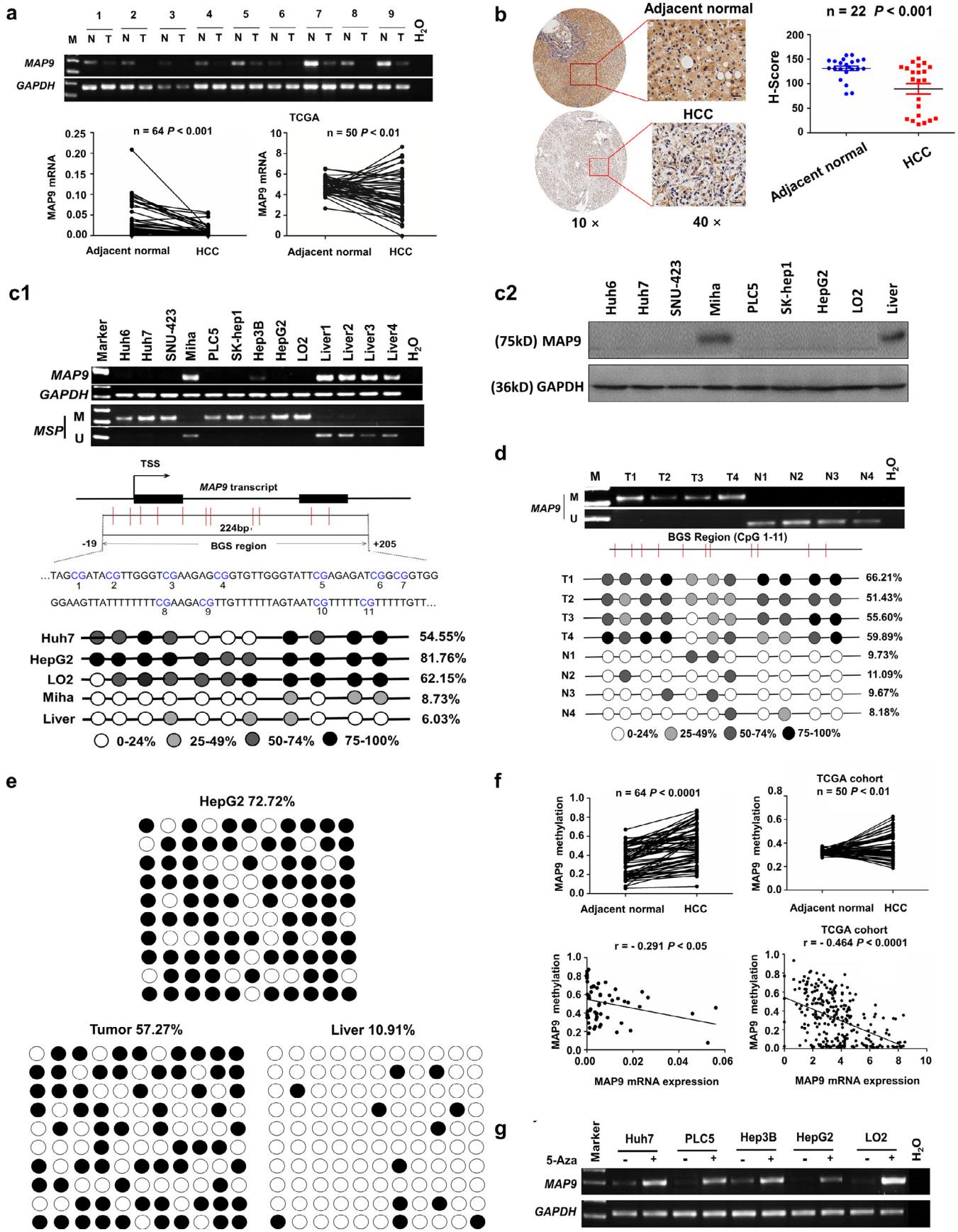

Fig. 1. MAP9 is silenced by promoter hypermethylation in liver cancer cells and tissue samples. (a) MAP9 mRNA level was dramatically decreased in liver tumour tissues (T) as compared with the paired non-tumour tissues (N) in our and TCGA cohorts. All data are normalized to adjacent normal and paired t-test was used to analyse the statistical difference between adjacent normal and HCC group. $n = 64$ for adjacent normal and HCC groups in our cohort. $P < 0.001$ (paired t-test) vs. adjacent normal. $n = 50$ for adjacent normal and HCC groups in TCGA cohort. $P < 0.01$ (paired t-test) vs. adjacent normal. (b) Representative images of IHC staining of MAP9 protein expression in HCC tissues. Scale bar: 75 μm. All

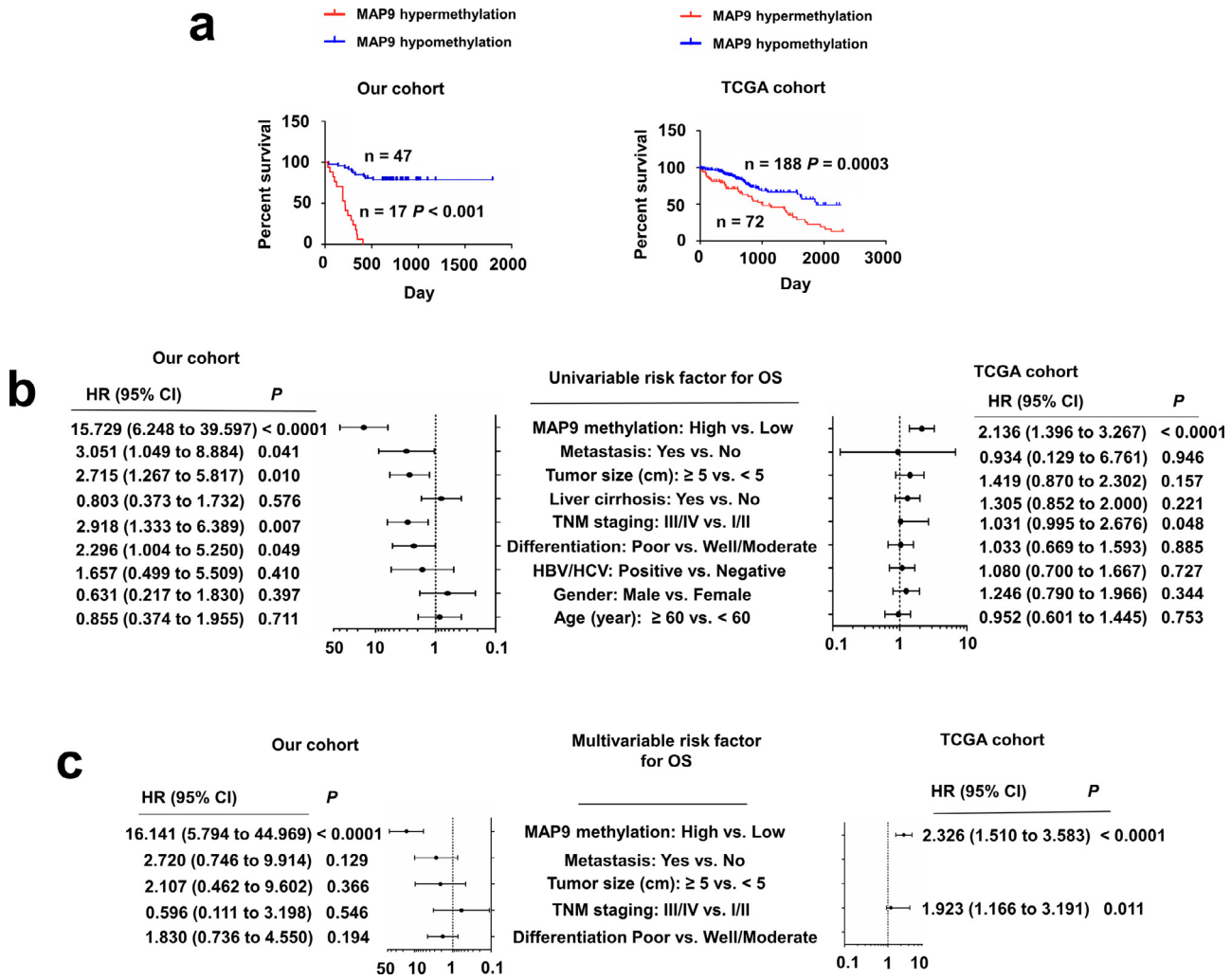

Fig. 2. MAP9 hypermethylation is associated with poor survival in patients with HCC. (a) Representative Kaplan-Meier plots of the association of MAP9 hypermethylation or hypomethylation with poor survival in HCC patients in our and TCGA cohorts. $P < 0.001$ (Kaplan–Meier analysis) vs. MAP9 hypomethylation in our cohort and $P = 0.0003$ (Kaplan-Meier analysis) vs. MAP9 hypomethylation in TCGA cohort. (b) Univariate Cox regression analysis of overall survival in HCC patients in our and TCGA cohorts. (c) Multivariate Cox regression of overall survival in HCC patients in our and TCGA cohorts.

transfected LO2 and HepG2 cell lines, while knockdown MAP9 promoted the colony formation ability in Miha cell line (Fig. 3b). In keeping with this, ectopic MAP9 expression suppressed cell viability in LO2 and HepG2 cell lines, while an inverse effect was observed in Miha cell line with MAP9 knockdown (Fig. 3c).

We analysed the effects of MAP9 on cell apoptosis by flow cytometry. Restoration of MAP9 expression caused an increase in the number of early and late apoptotic cells in LO2 and HepG2 cell lines. On the other hand, MAP9 knockdown diminished cell apoptosis in Miha cell lines (Fig. 3d). Accordingly, MAP9 enhanced the protein levels of activated form of caspase-9, caspase-7, caspase-3, and PARP in LO2 and HepG2 cell lines, while an inversed effect was observed in Miha cell line with MAP9 knockdown (Fig. 3d).

Additionally, ectopic MAP9 expression caused an elevated accumulation of LO2 and HepG2 cells in G1 phase and a corresponding decrease in the S phase, while knockdown of MAP9 induced a decrease of G1 phase population but an increase of S phase population in Miha cell line (Fig. 3e). Consistently, G1 phase gatekeepers $p27^{Kip1}$ and $p21^{Cip1}$ expression levels were enhanced but G1-S transition promoters Cyclin D1 and CDK4 were reduced by MAP9 overexpression, while the opposite results were presented by MAP9 knockdown (Fig. 3e). Therefore, our results indicated that MAP9 favored the apoptosis and prohibited the cell cycle in liver cell lines.

3.4. MAP9 inhibits liver cell migration and invasion

The effects of MAP9 on cell migration and invasion were further assessed. The migration capabilities were noticeably reduced by MAP9 overexpression in LO2 and HepG2 cells, but increased by

data are normalized to adjacent normal and paired t-test was used to analyse the statistical difference between adjacent normal and HCC group. $P < 0.001$ (paired *t*-test) vs. adjacent normal. (c-e) MAP9 mRNA and protein expression was silenced in liver cancer cell lines, and its downregulation showed a reverse correlation with promoter hypermethylation in liver cancer cell lines and tissue samples as determined by MSP and BGS analysis. (f) Promoter methylation level of MAP9 was substantially increased in HCC tissues as compared with adjacent non-tumour tissues, and had a negative association with its mRNA expression in HCC tissues. $n = 64$ for adjacent normal and HCC groups in our cohort. $P < 0.0001$ (paired *t*-test) vs. adjacent normal. $n = 50$ for adjacent normal and HCC groups in TCGA cohort. $P < 0.01$ (paired *t*-test) vs. adjacent normal. Pearson correlation analysis was used to analyse the correlation of MAP9 methylation with its mRNA expression in HCC. $r = -0.291$, $P < 0.05$ (Pearson correlation analysis) vs. MAP9 mRNA expression in our cohort, and $r = -0.464$, $P < 0.0001$ (Pearson correlation analysis)vs. MAP9 mRNA expression in TCGA cohort. (g) MAP9 mRNA level was restored in liver cancer cell lines after treatment with demethylating agent 5-Aza. M, methylation; U, unmethylation; TSS, transcription start site.

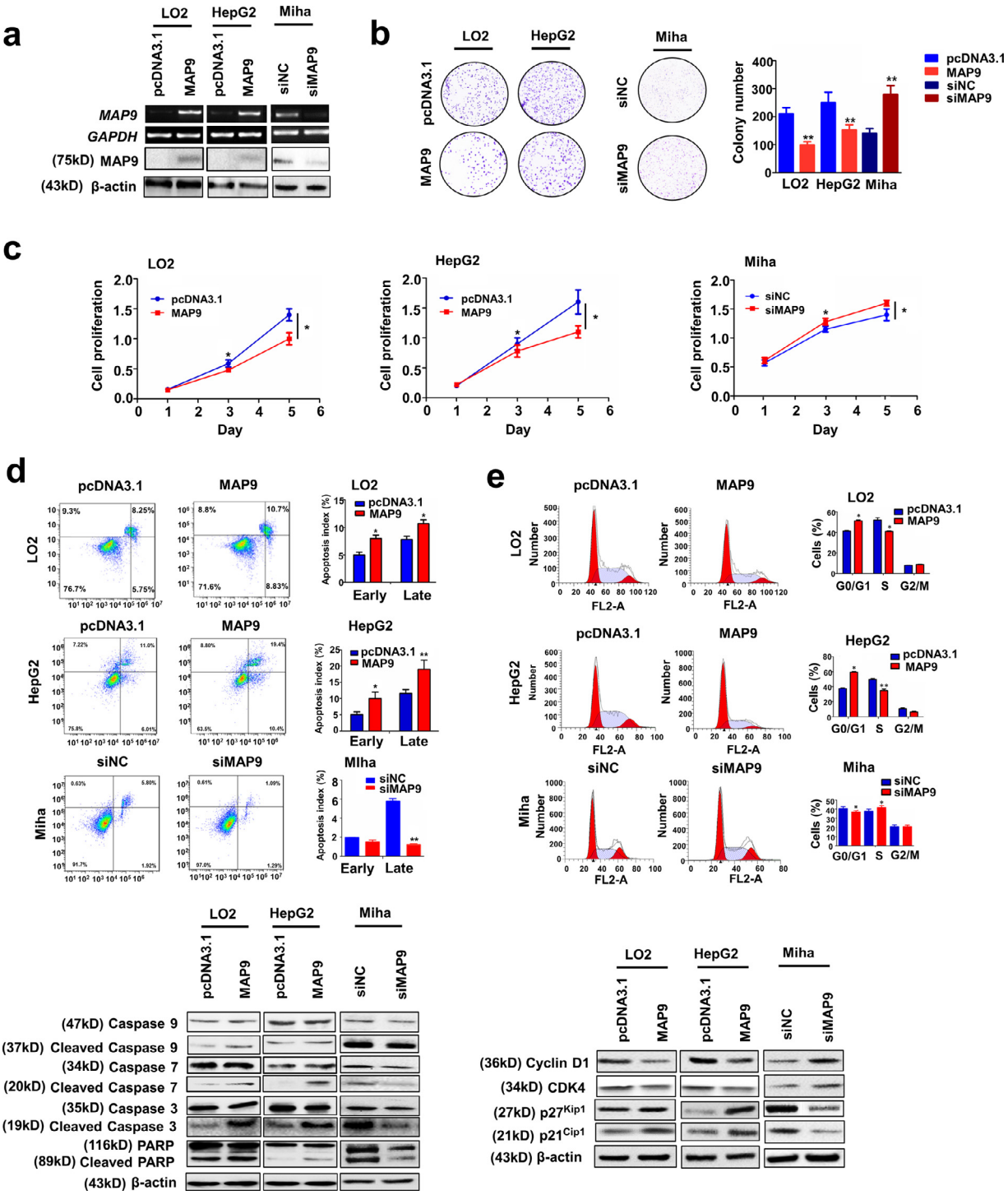

Fig. 3. MAP9 inhibits liver cancer cell growth by inducing cell apoptosis and blocking cycle progression. (a) The transfection efficiency of MAP9 plasmid in LO2 and HepG2 cell lines and siMAP9 in Miha cell line was determined by RT-PCR and Western blot analysis. (b) MAP9 overexpression suppressed colony formation in LO2 and HepG2 cell lines, but knockdown of MAP9 reversed these effects. All data are normalized to the control. $n = 3$ for each group, $^{**}P < 0.01$ (unpaired t-test) vs. control. (c) Cell viability was decreased by transfection with MAP9 in HepG2 and LO2 cell lines, but increased by knockdown of MAP9 in Miha cell line. All data are normalized to the control. $n = 3$ for each group, $^{*}P < 0.05$ (unpaired t-test) vs. control. (d) MAP9 induced cell apoptosis by flow cytometry analysis of cells stained with annexin V/7-AAD, while knockdown of MAP9 reduced cell apoptosis (upper panel). MAP9 increased the protein levels of the active forms of caspase-9, −7 and −3 and PARP in LO2 and HepG2 cell lines, but knockdown of MAP9 showed the opposite effects in Miha cell line by Western blot analysis (lower panel). All data are normalized to the control. $n = 3$ for each group, $^{*}P < 0.05$ and $^{**}P < 0.01$ (unpaired t-test) vs. control. (e) MAP9 increased the number of cells in G1 phase, but decreased the number of cells in S phase by flow cytometry analysis in LO2 and HepG2 cells, while knockdown of MAP9 promoted the cell cycle at the G1-S transition in Miha cell (upper panel). MAP9 downregulated cyclinD1 and CDK4 expression, and upregulated $p27^{Kip1}$ and $p21^{Cip1}$ expression by Western blot analysis, but knockdown of MAP9 had the opposite effect (lower panel). All data are normalized to the control. $n = 3$ for each group, $^{*}P < 0.05$ and $^{**}P < 0.01$ (unpaired t-test) vs. control.

knockdown of MAP9 in Miha cells (Fig. 4a) by wound-healing assay. The similar results were presented by Transwell migration assay (Fig. 4b). In addition, the invasive potential was dramatically weakened by MAP9 overexpression in LO2 and HepG2 cells, but reinforced by knockdown of MAP9 in Miha cells (Fig. 4c) by Transwell invasion assay.

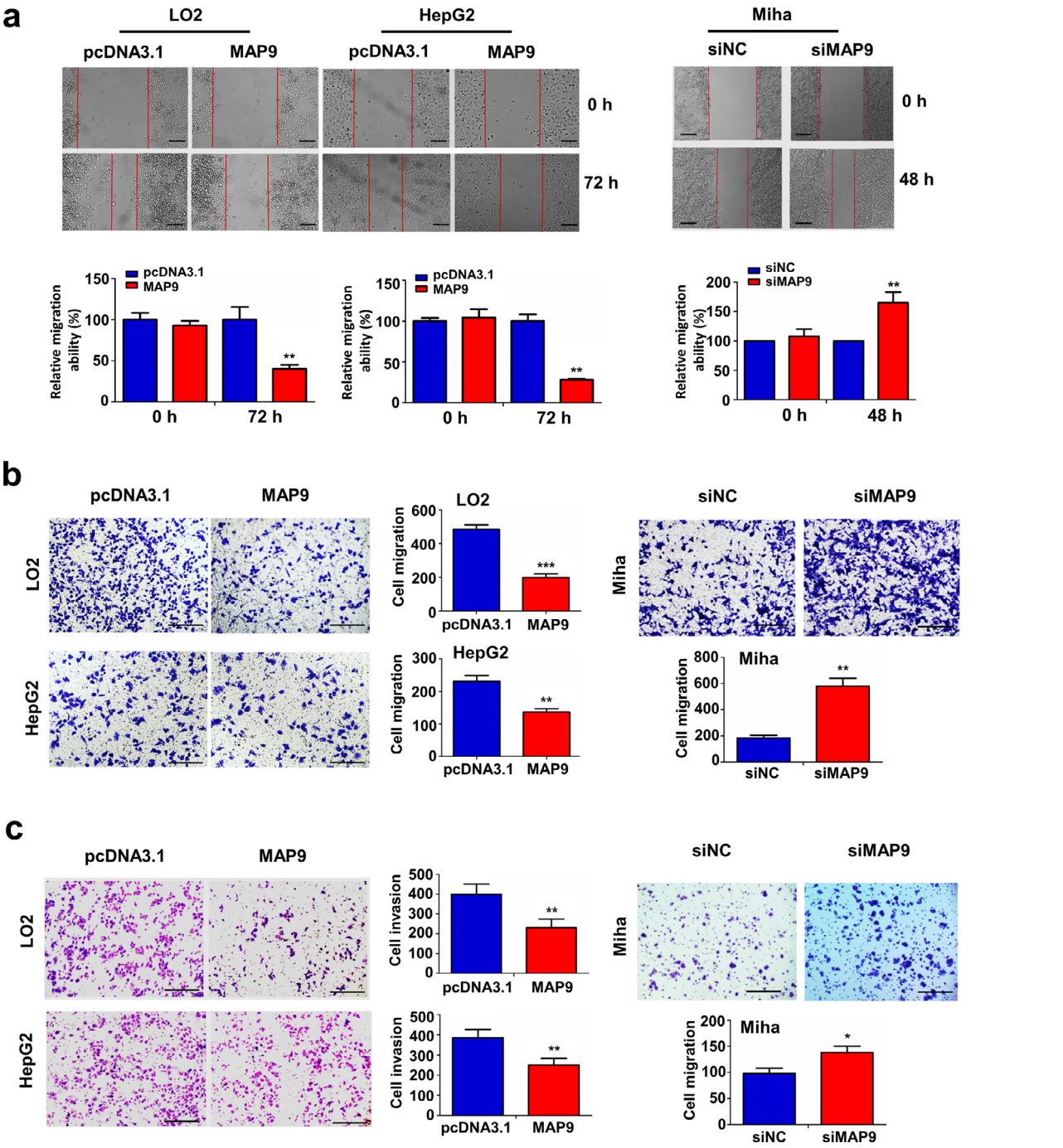

Fig. 4. MAP9 inhibits liver cancer cell migration and invasion. (a, b) Wound-healing and Transwell migration assays were performed to investigate the effects of MAP9 on cell migration capabilities in liver cancer cell lines. (a) Scale bar: 75 μm. All data are normalized to the control. $n = 3$ for each group, $^{**}P < 0.01$ (unpaired t-test) vs. the control. (b) Scale bar: 150 μm. All data are normalized to the control. $n = 3$ for each group, $^{**}P < 0.01$ and $^{***}P < 0.001$ (unpaired t-test) vs. the control. (c) Transwell invasion assays were conducted to observe the effects of MAP9 on cell invasive potential in liver cancer cell lines. Scale bar: 150 μm. All data are normalized to the control. $n = 3$ for each group, $^{*}P < 0.05$ and $^{**}P < 0.01$ (unpaired t-test) vs. the control.

3.5. Hepatocyte-specific knockout of MAP9 accelerates DEN-induced hepatocarcinogenesis

To confirm the functional significance of MAP9 in HCC formation, we constructed *Map9* conditional hepatocyte-specific knockout mice ($MAP9^{\Delta/\Delta hep}$) (Fig. 5a). $MAP9^{\Delta/\Delta hep}$ and WT mice administered with a single dose of DEN at 2 weeks of age. At 30 weeks of age, mice were sacrificed and the liver tissues were analysed. The absence of *Map9* mRNA and protein in the liver tissues of $MAP9^{\Delta/\Delta}$ mice was confirmed by RT-PCR and Western blot analysis (Fig. 5b). $MAP9^{\Delta/\Delta hep}$ mice developed significant more tumours (100%, 5/5) as compare with WT mice (40%, 4/10), accompanied with hepatocyte dysplasia, liver cell injury, necrosis and inflammatory cell infiltration (Fig. 5c). $MAP9^{\Delta/\Delta hep}$ mice displayed the increased liver weight, tumour volume and tumour number (Fig. 5d). Liver tumours derived from $MAP9^{\Delta/\Delta hep}$ mice exhibited a higher Ki-67 score (15.20 ± 3.44) but a lower apoptosis index (5.61 ± 0.77) compared with the WT mice (7.36 ± 1.65; 2.08 ± 0.36) (Fig. 5e). These indicated that hepatocyte-specific MAP9 knockout promoted DEN-induced HCC formation.

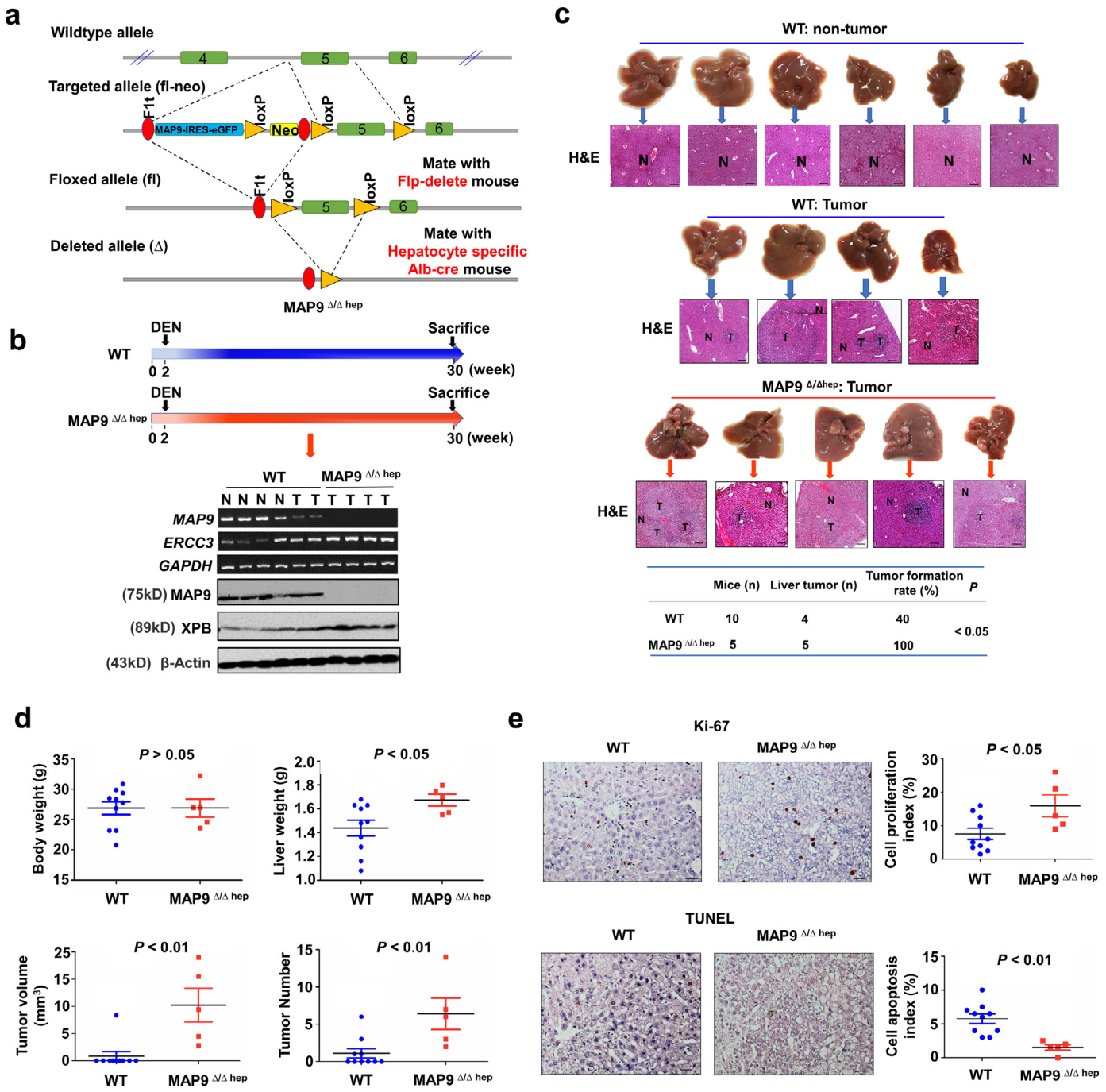

Fig. 5. Hepatocyte-specific knockout of MAP9 accelerates DEN-induced hepatocarcinogenesis. (a) Scheme for the generation of hepatocyte-specific MAP9 knockout (MAP9 $^{\Delta/\Delta hep}$) mice. (b) Experimental design of DEN-induced liver tumour model in MAP9 $^{\Delta/\Delta hep}$ and WT mice (upper panel), and RT-PCR and Western blot validation of MAP9 deletion and ERCC3/XPB expression in liver tumour tissues from MAP9 $^{\Delta/\Delta hep}$ and WT mice (lower panel). (c) H&E staining of the live tissues, and comparison of the formation rate of liver tumors in MAP9 $^{\Delta/\Delta hep}$ and WT mice. T: tumour tissues; N: non-tumour tissues. Scale bar: 300 μm. All data are normalized to the WT group. $P < 0.05$ (Chi square test) vs. the WT group. (d) Comparison of the body weight, tumour weight, tumour volume and tumour number in MAP9 $^{\Delta/\Delta hep}$ and WT mice. All data are normalized to the WT group. $P < 0.05$ and $P < 0.01$ (unpaired *t*-test) vs. the WT group. (e) Ki-67 staining and TUNEL analysis of cell proliferation and apoptosis index in MAP9 $^{\Delta/\Delta hep}$ and WT mice. Scale bar: 150 μm. All data are normalized to the WT group. $P < 0.05$ and $P < 0.01$ (unpaired *t*-test) vs. the WT group.

3.6. Knockout of MAP9 causes a spontaneous liver hyperplastic nodule in mice

Having observed the effect of MAP9 $^{\Delta/\Delta hep}$ on DEN-induced hepatocarcinogenesis, we investigated whether MAP9 $^{\Delta/\Delta}$ could induce a spontaneous HCC formation. At 40 weeks of age, MAP9 $^{\Delta/\Delta}$ mice were sacrificed and the liver tissues were examined. MAP9 was confirmed to be deleted in liver tissues of MAP9 $^{\Delta/\Delta}$ mice (Fig. 6a). MAP9 $^{\Delta/\Delta}$ mice developed a spontaneous liver hyperplastic nodule, which was confirmed histologically as hepatocyte dysplasia with inflammatory cell infiltration (Fig. 6b). When compared with the WT mice, MAP9 $^{\Delta/\Delta}$ mice displayed an increased Ki-67 score (15.61 ± 0.71) but a decreased cell apoptosis index (2.58 ± 0.11) in liver tissues compared with the WT mice (10.50±1.04; 6.17±0.73) (Fig. 6c). There were no significant differences in body weight and liver weight between MAP9 $^{\Delta/\Delta}$ and WT mice (Supplementary Fig. S4).

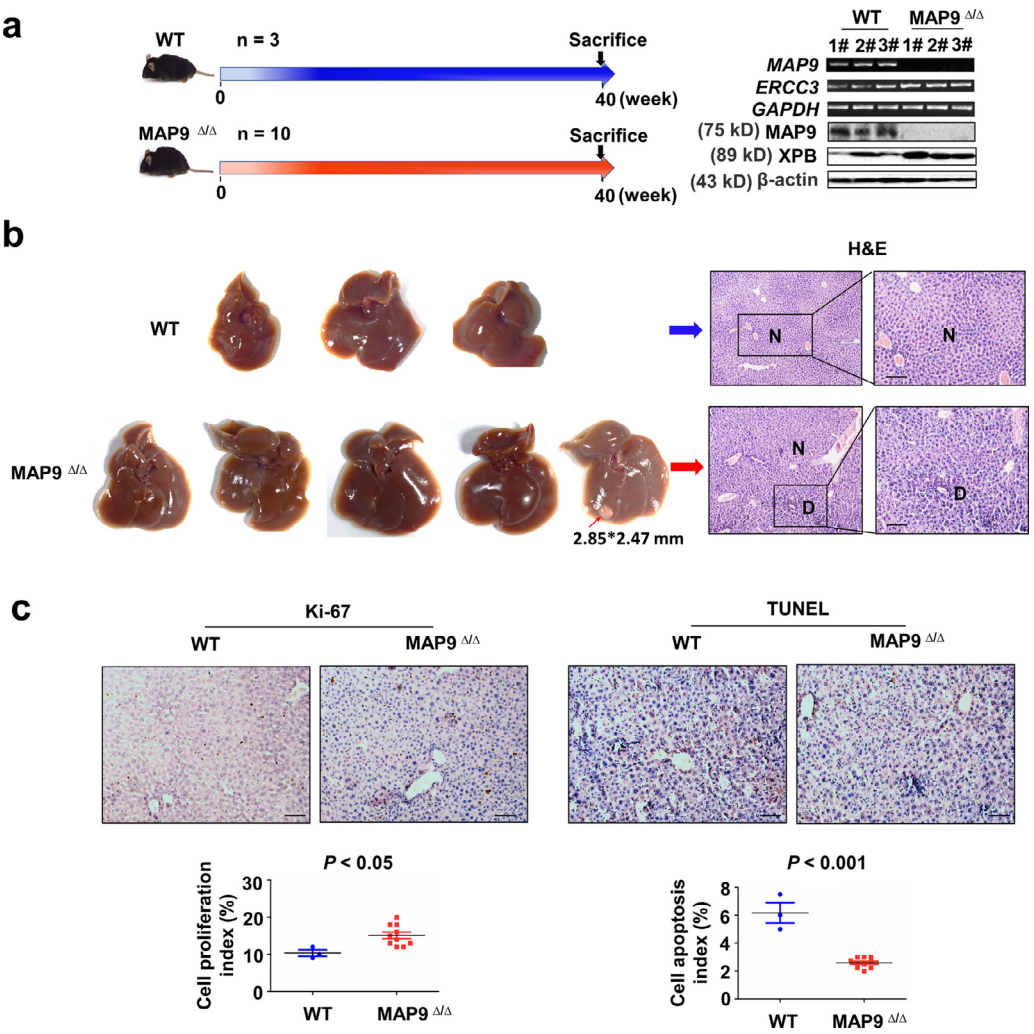

Fig. 6. Knockout of MAP9 causes a spontaneous liver hyperplastic nodule in mice. (a) Experimental design of MAP9$^{\Delta/\Delta}$ and WT mice (left panel), and RT-PCR and Western blot validation of MAP9 deletion and ERCC3/XPB expression in liver tissues from MAP9$^{\Delta/\Delta}$ and WT mice (right panel). (b) Representative images and H&E staining of the live tissues in MAP9 $^{\Delta/\Delta}$ and WT mice. D: dysplastic tissues; N: non-tumour tissues. Scale bar: 150 μm. (c) Ki-67 staining and TUNEL analysis of cell proliferation and apoptosis index in MAP9 $^{\Delta/\Delta}$ and WT mice. Scale bar: 150 μm. All data are normalized to the WT group. $P < 0.05$ and $P < 0.001$ (unpaired *t*-test) vs. the WT group.

3.7. ERCC3 is identified as a negative regulator of MAP9

At 12 weeks of age, MAP9 $^{\Delta/\Delta}$ and WT littermates were sacrificed and the liver tissues were analysed. MAP9 was confirmed to be deleted in liver tissues of MAP9 $^{\Delta/\Delta}$ mice, which showed decreased body weight and liver weight compared with the WT mice (Fig. 7a). We performed the hierarchical clustering analysis and identified about 30 aberrantly expressed genes in liver tissues from MAP9 $^{\Delta/\Delta}$ and WT mice by using a cancer pathway PCR array (Fig. 7b). Amongst them, several upregulated genes in MAP9 $^{\Delta/\Delta}$ group formed a gene co-expressed cluster, including *Ercc3, Pinx1, Foxo2, Ercc5, Lig4, B2m, Uqcrfs1, Xrcc4, Gadd45g, Ldha, Cdc20* and *Serpinb2*. Furthermore, Gene Set Enrichment Analysis (GSEA) was used to assess the enrichment of Kyoto encyclopedia of Genes and Genomes (KEGG) pathways. According to the Normalized Enrichment Score (NES) value and *P* value, a nucleotide excision repair (NER) pathway was identified to be most significantly associated with the phenotype of MAP9 deletion (Fig. 7c). Key genes in NER pathway had the core enrichment, such as *Ercc3, Xrcc4, Ercc5, Lig4*, of which *Ercc3* exhibited the highest rank metric score and might act a critical role in liver pathogenesis in MAP9 $^{\Delta/\Delta}$ mice (Fig. 7c).

We further investigated the expression of ERCC3 and xeroderma pigmentosum complementation group B (XPB, the DNA helicase encoded by ERCC3) in MAP9 $^{\Delta/\Delta}$ mice and liver cells. MAP9 ablation increased the expression of ERCC3 mRNA and XPB protein levels in mice liver tissues, whereas MAP9 overexpression reduced ERCC3 mRNA and XPB protein expression in HepG2 and LO2 cell lines (Fig. 7d). Immunofluorescence analysis showed that MAP9 overexpression was localized in the cytoplasm while XPB was localized in the nucleus in HepG2 and LO2 cell lines (Fig. 7e). We also found that ERCC3 expression was upregulated in HCC tissues as compared with adjacent non-tumour tissues and harboured a negative correlation with MAP9 expression in HCC samples (Supplementary Fig. S5). Moreover, ERCC3 was upregulated in 50 paired and 371 unpaired HCC tissues as compared with adjacent non-tumour tissues from TCGA cohort (Supplementary Fig. S6a). In contrary to MAP9 expression, the patients with ERCC3 high expression possessed a shorter survival (Supplementary Fig. S6b), as compared with those with ERCC3 low expression. Univariate and multivariate Cox regression analysis unveiled that ERCC3 high expression was an independent prognostic factor of poor survival in HCC patients (Supplementary Table S7).

3.8. ERCC3 counteracts the tumour suppressive effects of MAP9 in HCC cells

To evaluate whether MAP9 induces a tumour suppression through regulating ERCC3, we transfected ERCC3, MAP9, or co-transfected

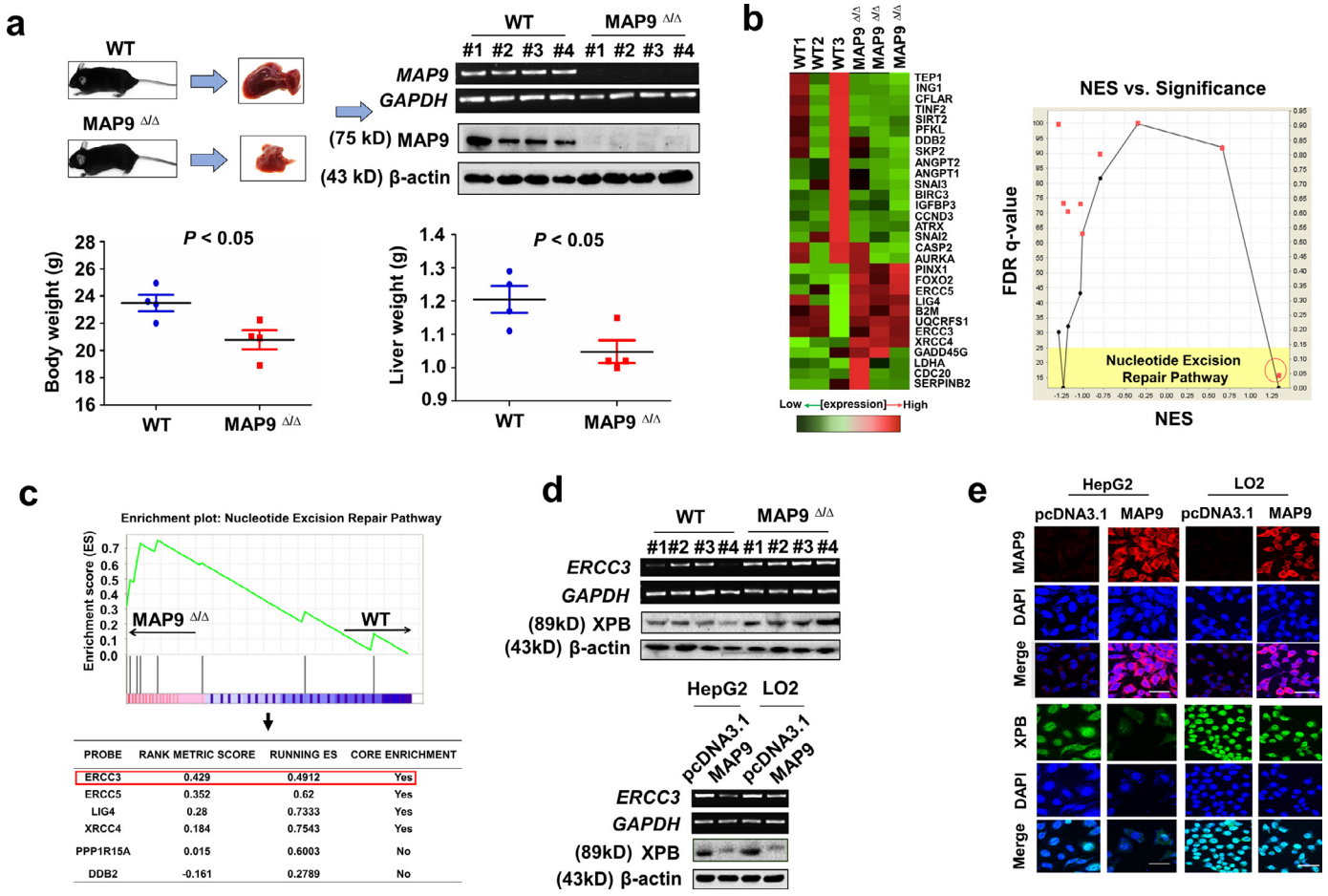

Fig. 7. ERCC3 is identified as a negative regulator of MAP9 in liver tissues and cell lines. (a) RT-PCR and Western blot validation of MAP9 deletion in liver tissues in MAP9 $^{\Delta/\Delta}$ mice and WT mice (upper panel). Body weight and liver weight were decreased in MAP9 $^{\Delta/\Delta}$ mice as compared with WT mice (lower panel). All data are normalized to the WT group. $n = 4$ for each group, $P < 0.05$ (unpaired t-test) vs. the WT group. (b) Heat map of the cancer pathway PCR array using the live tissues from MAP9 $^{\Delta/\Delta}$ mice and WT mice (left panel). GSEA and NES assessment of the enrichment of NER pathway associated with the phenotype of MAP9 deletion in liver tissues (right panel). (c) The genes in NER pathway had core enrichment and Ercc3 had the highest rank metric score. (d) RT-PCR and Western blot analysis of the effects of MAP9 knockout on ERCC3/XPB expression in liver tissues (upper panel) and cell lines (lower panel). (e) Representative images under confocal microscopy demonstrated the effects of MAP9 on the nuclear accumulation of XPB in LO2 and HepG2 cell lines. Scale bar: 75 μm.

ERCC3 and MAP9 in LO2 and HepG2 cell lines respectively. We found that ERCC3 overexpression promoted cell proliferation (Fig. 8a, b), increased the number of colonies (Fig. 8c) and boosted cell invasion (Fig. 8d) in LO2 and HepG2 cell lines. The inhibitory effects of MAP9 on cell proliferation, colony formation and cell invasion in LO2 and HepG2 cell lines were attenuated by ERCC3 (Fig. 8b–d). These results collectively indicated that the tumour suppressive function of MAP9 in HCC was at least in part depending on the reduction of ERCC3 expression.

4. Discussion

In this study, we first demonstrated that MAP9 was frequently silenced in liver cancer cell lines and tissue samples due to its promoter hypermethylation. The clinical significance of MAP9 methylation or its low expression in patients with HCC was then assessed. MAP9 hypermethylation or its low expression (Fig. 2, Supplementary Fig. S2, Table S4-6) was an independent risk factor of poor survival and tumour recurrence in patients with HCC. The patients with MAP9 hypermethylation or low expression (Supplementary Fig. S7) conferred a shorter survival and a higher tumour recurrence. In light of the diversity in tumour proliferating status, aggressive potential and therapeutic outcomes, the prognosis of HCC patients varies. Some patients in early stage with MAP9 hypermethylation or its low expression were subjected to an unfavourable prognosis. Identification of more promising biomarkers may favour the assessment of the outcome of HCC patients. DNA promoter methylation has been reported as the potential predictors of HCC patients [3, 17]. This finding inferred MAP9 hypermethylation as a novel prognostic biomarker in patients with HCC.

The functional importance of MAP9 in HCC was investigated. Ectopic expression of MAP9 suppressed cell viability and colony formation, whereas knockdown of MAP9 showed an opposite effect in vitro. To confirm the tumour suppressive role of MAP9 in HCC, we generated MAP9 conditional knockout model. Hepatocyte-specific deletion of MAP9 in mice facilitated DEN-induced HCC progression. Moreover, MAP9 knockout mice developed spontaneously liver dysplastic nodule. These findings confirmed MAP9 was a novel tumour suppressor gene in HCC.

The mechanisms of MAP9 as a tumour suppressor gene in HCC was investigated. The tumour suppressive function of MAP9 was mediated by inducing cell apoptosis and suppressing cell proliferation and cell cycle progression. MAP9 induced cell apoptosis by activating intrinsic and extrinsic apoptosis pathway, causing activation in caspase-9 and its downstream effectors caspase-3, caspase-7 and PARP. MAP9 blocked cell-cycle transition at G1-S phase, associated with decreased expression of cyclin D1 and CDK4 as well as increased expression of $p27^{Kip1}$ and $p21^{Cip1}$. Cyclin D1/CDK4 complex is engaged in control of cell proliferation during G1 phase, and $p21^{Cip1}$ and $p27^{Kip1}$ can inhibit its activity [18]. MAP9 mediated cell

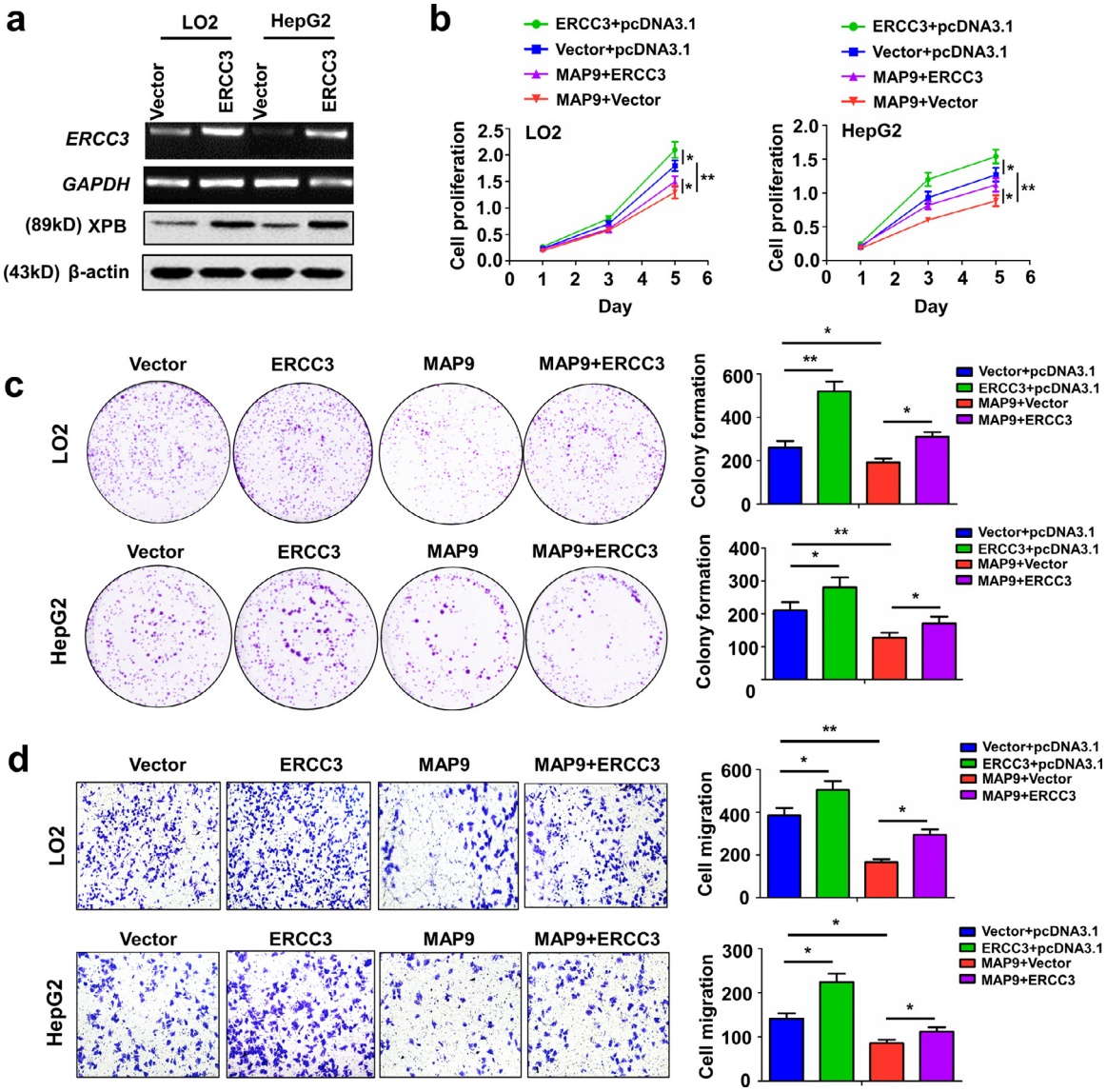

Fig. 8. Ectopic expression of ERCC3 reverses the anti-tumour effects of MAP9 in HCC cells. (a) Overexpression of ERCC3 in LO2 and HepG2 cell lines was determined by RT-PCR. (b-d) MTT, colony formation and Transwell assays were used to assess the cell viability, colony number and cell invasive potential after co-transfection with ERCC3 and MAP9 plasmids in LO2 and HepG2 cell lines. All data are normalized to the control. $n = 3$ for each group, $^{*}P < 0.05$ and $^{**}P < 0.01$ (One-way ANOVA) vs. control.

apoptosis, cell proliferation and cell cycle progression in HCC cell lines were confirmed in a MAP9 knockout mouse model. Moreover, MAP9 inhibited the migration and invasion potential of HCC cells. Tumour metastasis is a predominant cause of cancer-related deaths [19]. This result further confirmed the role of MAP9 as a tumour suppressor gene in HCC.

To gain insights into the mechanisms by which MAP9 functioned as a tumour suppressor in HCC, we applied a gene expression profiling assay in liver tissues from MAP9 knockout and WT mice. We identified that NER pathway as one of the critical pathways was involved in MAP9 functional regulation in liver. NER, the most flexible of the DNA repair pathways in response to the multiformity of DNA lesions, executes the excision of the damaged DNA fragment and synthesis of a new DNA strand portion [20]. Deregulation of NER signalling has been reported in a variety of malignancies [21-24]. Here we demonstrated that NER signalling was involved in the liver pathogenesis in MAP9 knockout mice. We further revealed that ERCC3 was a core-enriched gene in NER pathway regulated by MAP9 in HCCs. Enhanced ERCC3/XPB expression was demonstrated in liver tissues of $MAP9^{\Delta/\Delta}$ mice. We discovered that ERCC3 harboured an increased expression, depicted a negative correlation with MAP9 expression and acted as an independent prognostic factor of poor survival in HCC patients. Besides, appreciable decrease in ERCC3/XPB expression or nuclear aggregation was caused by MAP9, but a substantial increase was shown in liver tumours in $MAP9^{\Delta/\Delta hep}$ mice. Re-expression of ERCC3 promoted cell growth and invasion, and abrogated the tumour suppressive effects of MAP9. These data collectively indicated that ERCC3 was required for MAP9 deficiency induced HCC. As a core gene in NER pathway, ERCC3 may influences the aggressive phenotype of liver cancer cells through DNA damage. We have recently reported that MAP9 acted as a microtubule stabilizer and MAP9 loss caused chromosomal instability especially in $MAP9^{-/-}p53^{+/-}$ mice [25]. Others have reported that MAP9 directly interacts with and stabilizes p53 [12], which could regulate NER pathway and contribute to DNA repair [26]. A direct interaction of p53 with ERCC3 was demonstrated in hepatitis C virus infection [27]. Therefore, MAP9 may regulate ERCC3 in NER pathway through upregulating p53. Further studies need to be conducted to confirm the exact mechanistic interplay of MAP9 on ERCC3 regulation.

In conclusion, we identified for the first time that MAP9 is a novel tumour suppressor gene in HCC. MAP9 exerts a tumour suppressive function by downregulating ERCC3/XPB expression and serves as an independent prognostic factor in HCC patients.

Declaration of Competing Interest

All authors declare no conflicts of interests.

Funding sources

This work was supported by National Key R&D Program of China (2017YFE0190700), Hong Kong Scholars Program (XJ2015033), RGC-CRF Hong Kong (C4041-17GF; C7026-18G; C7065-18G), Vice-Chancellor's Discretionary Fund CUHK, and Shenzhen Virtual University Park Support Scheme to CUHK Shenzhen Research Institute. The sponsors of the study had no role in study design, data collection, data analysis, data interpretation, or writing of the report. The corresponding author had full access to all the data in the study and had final responsibility for the decision to submit for publication.

Author's contribution

Conception and design: JY.

Performed the research and data collection: JZ, JZH, YQZ, LYZ, CGL, YFZ and HW.

Data analysis and interpretation: JZ, JZH, YQZ, XZ, LYZ and HW.

Drafted the manuscript: JZ, XZ and JY.

All authors read and approved the final version of the manuscript.

Supplementary materials

Supplementary material associated with this article can be found in the online version at doi:10.1016/j.ebiom.2020.102701.

References

[1] Siegel RL, Miller KD, Jemal A. Cancer statistics, 2018. CA Cancer J Clin 2018;68:7–30.
[2] Chen W, Zheng R, Zhang S, Zeng H, Xia C, Zuo T, et al. Cancer incidence and mortality in China, 2013. Cancer Lett 2017;401:63–71.
[3] Yu J, Tao Q, Cheung KF, Jin H, Poon F, Wang X, et al. Epigenetic identification of ubiquitin carboxyl-terminal hydrolase L1 as a functional tumour suppressor and biomarker for hepatocellular carcinoma and other digestive tumors. Hepatology 2008;48:508–18.
[4] Zhu H, Wu K, Yan W, Hu L, Yuan J, Dong Y, et al. Epigenetic silencing of DACH1 induces loss of transforming growth factor-β1 antiproliferative response in human hepatocellular carcinoma. Hepatology 2013;58:2012–22.
[5] Ramkumar A, Jong BY, Ori-McKenney KM. ReMAPping the microtubule landscape: how phosphorylation dictates the activities of microtubule-associated proteins. Dev Dyn 2018;247:138–55.
[6] Gylfe AE, Kondelin J, Turunen M, Ristolainen H, Katainen R, Pitkänen E, et al. Identification of candidate oncogenes in human colorectal cancers with microsatellite instability. Gastroenterology 2013;145:540–3 e22.
[7] Jiang YY, Shang L, Shi ZZ, Zhang TT, Ma S, Lu CC, et al. Microtubule-associated protein 4 is an important regulator of cell invasion/migration and a potential therapeutic target in esophageal squamous cell carcinoma. Oncogene 2016;35:4846–56.
[8] Barbieri CE, Baca SC, Lawrence MS, Demichelis F, Blattner M, Theurillat JP, et al. Exome sequencing identifies recurrent SPOP, FOXA1 and MED12 mutations in prostate cancer. Nat Genet 2012;44:685–9.
[9] Saffin JM, Venoux M, Prigent C, Espeut J, Poulat F, Giorgi D, et al. ASAP, a human microtubule-associated protein required for bipolar spindle assembly and cytokinesis. Proc Natl Acad Sci U S A 2005;102:11302–7.
[10] Venoux M, Delmouly K, Milhavet O, Vidal-Eychenié S, Giorgi D, Rouquier S. Gene organization, evolution and expression of the microtubule-associated protein ASAP (MAP9). BMC Genomics 2008;9:406.
[11] Fontenille L, Rouquier 2 S, Lutfalla G, Giorgi D. Microtubule-associated protein 9 (Map9/Asap) is required for the early steps of zebrafish development. Cell Cycle 2014;13:1101–14.
[12] Basbous J, Knani D, Bonneaud N, Giorgi D, Brondello JM, Rouquier S. Induction of ASAP (MAP9) contributes to p53 stabilization in response to DNA damage. Cell Cycle 2012;11:2380–90.
[13] Rouquier S, Pillaire MJ, Cazaux C, Giorgi D. Expression of the microtubule-associated protein MAP9/ASAP and its partners Aurka and PLK1 in colorectal and breast cancers. Dis Markers 2014;2014:798170.
[14] Sun W, Zhang Y, Wong KC, Liu K, Yang Y, Wu B, et al. Increased expression of GATA Zinc finger domain containing 1 via gene amplification promotes liver cancer by directly inducing PRL3. Hepatology 2018;67:2302–19.
[15] Farley FW, Soriano P, Steffen LS, Dymecki SM. Widespread recombinase expression using FLPeR (flipper) mice. Genesis 2000;28:106–10.
[16] Postic C, Shiota M, Niswender KD, Jetton TL, Chen Y, Moates JM, et al. Dual roles for glucokinase in glucose homeostasis as determined by liver and pancreatic beta cell-specific gene knock-outs using CRE recombinase. J Biol Chem 1999;274:305–15.
[17] Villanueva A, Portela A, Sayols S, Battiston C, Hoshida Y, Méndez-González J, et al. DNA methylation-based prognosis and epidrivers in hepatocellular carcinoma. Hepatology 2015;61:1945–56.
[18] Serrano M, Hannon GJ, Beach D. A new regulatory motif in cell-cycle control causing specific inhibition of cyclin D/CDK4. Nature 1993;366:704–7.
[19] Robinson DR, Wu YM, Lonigro RJ, Vats P, Cobain E, Everett J, et al. Integrative clinical genomics of metastatic cancer. Nature 2017;548:297–303.
[20] Zhou BB, Elledge SJ. The dna damage response: putting checkpoints in perspective. Nature 2000;408:433–9.
[21] Szalat R, Samur MK, Fulciniti M, Tai YT, Shammas MA, Anderson KC, et al. Nucleotide excision repair is a potential therapeutic target in multiple myeloma. Leukemia 2018;32:111–9.
[22] Fleming ND, Agadjanian H, Nassanian H, Miller CW, Orsulic S, Karlan BY, et al. Xeroderma pigmentosum complementation group C single-nucleotide polymorphisms in the nucleotide excision repair pathway correlate with prolonged progression-free survival in advanced ovarian cancer. Cancer 2012;118:689–97.
[23] Lu B, Li J, Gao Q, Yu W, Yang Q, Li X. Laryngeal cancer risk and common single nucleotide polymorphisms in nucleotide excision repair pathway genes ERCC1, ERCC2, ERCC3, ERCC4, ERCC5 and XPA. Gene 2014;542:64–8.
[24] Jung SW, Park NH, Shin JW, Park BR, Kim CJ, Lee JE, et al. Polymorphisms of DNA repair genes in Korean hepatocellular carcinoma patients with chronic hepatitis B: possible implications on survival. J Hepatol 2012;57:621–7.
[25] Wang S, Huang J, Li C, Zhao L, Wong CC, Zhai J, et al. MAP9 loss triggers chromosomal instability, initiates colorectal tumorigenesis, and is associated with poor survival of patients with colorectal cancer. Clin Cancer Res 2019 Oct 29. doi: 10.1158/1078-0432.CCR-19-1611.
[26] Seo YR, Jung HJ. The potential roles of p53 tumor suppressor in nucleotide excision repair (NER) and base excision repair (BER). Exp Mol Med 2004;36:505–9.
[27] Qadri I, Iwahashi M, Simon F. Hepatitis C virus NS5A protein binds TBP and p53, inhibiting their DNA binding and p53 interactions with TBP and ERCC3. Biochim Biophys Acta 2002;1592:193–204.